Journal of Applied Polymer Science

Influence of the amorphous phase molecular mobility on impact and tensile properties of polyamide 6,6

Agustín Rios de Anda,* Louise-Anne Fillot,† Didier R. Long, Paul Sotta

Laboratoire Polymères et Matériaux Avancés, CNRS/Solvay UMR 5268, Solvay in Axel'one, 87 rue Frères Perret, 69192, Saint Fons Cedex, France

*Present address: CERMAV-Centre de Recherche sur les Macromolécules Végétales, 601 avenue de la Chimie, Domaine Universitaire de Grenoble - Saint Martin d'Hères, BP53 38041, Grenoble Cedex 9, France

†Present address: Solvay Engineering Plastics, Avenue Ramboz-BP 64, 69192, Saint-Fons Cedex

Correspondence to: P. Sotta (E-mail: paul.sotta-exterieur@solvay.com)

ABSTRACT: In this work, the relationship between molecular mobility of polyamide 6,6 amorphous phase and mechanical properties is studied. PA66 formulations having different glass transition temperatures (T_g) obtained by additivation, chemical modification of the polyamide chains, and/or water conditioning at different hygrometry levels, are considered. The main emphasis is put on the impact strength, as measured by instrumented Charpy impact tests over a broad temperature range. It is observed that the brittle-tough transition temperature $T_{B/T}$ is closely correlated with the T_g of the samples rather than to the β secondary relaxation. © 2016 Wiley Periodicals, Inc. J. Appl. Polym. Sci. **2016**, *133*, 43457.

KEYWORDS: mechanical properties; polyamides; spectroscopy

Received 26 November 2015; accepted 20 January 2016

DOI: 10.1002/app.43457

INTRODUCTION

Polyamides are semicrystalline polymers possessing a crystalline, solvent-tight phase and an amorphous phase, wherein solvent diffusion and sorption primarily occur. Since the crystalline ratio of polyamides is relatively low (between 35 and 40 wt % typically),[1] the properties of the amorphous phase may have a major influence on the overall behavior of these polymers. Polyamides possess a physical network of amide–amide hydrogen (H) bonds in both the amorphous and the crystalline phases. The existence of this network, especially in the amorphous phase, gives polyamides good mechanical and thermal properties.[2–8]

It has been observed in the literature[9–12] that the crystalline phase, specifically the crystalline ratio,[9,10] the size of the crystallites,[11] and the crystalline phase structure[12] have an effect on the mechanical properties of polyamides. It has been observed that the stiffness and the yield stress of PA6,6 increase, and that tensile strength of PA6,10 increases, when the crystalline ratio increases.[9] Also, it was observed that the yield strength of PA6,6 increases as the spherulites size decreases.[11] Furthermore, Miri *et al.*[12] have studied the effect of the crystalline structure on the tensile properties of PA6. They have observed that the stiffer samples were those containing the denser α crystalline form, followed by those containing the γ form and then those containing the nonstable β form. The effect of temperature on the tensile properties of PA6 has been studied by Shan *et al.*[13] It was observed that the yield stress depends linearly on temperature far enough below T_g, while this variation changed on approaching T_g. The influence of the crystalline structure on tensile properties, noticeably on the appearance of a double yielding phenomenon in some occurrences, was emphasized.[13]

The brittle-tough transition is an essential notion when dealing with ultimate mechanical properties of engineering plastics such as polyamides. The brittle-tough transition temperature $T_{B/T}$ may be defined in various ways. First, it can be defined from uniaxial stretching experiments, as the temperature at which failure occurs exactly at the yield stress. Above this temperature, failure occurs in the viscoplastic regime, beyond the yield stress, while below $T_{B/T}$, it occurs in the elastic or anelastic regime and a yield stress cannot be defined. In polymers, as well as other materials such as metals, the brittle-tough transition temperature $T_{B/T}$ is not an intrinsic property of the materials. It depends on the strain rate, and generally increases as the strain rate increases, being generally related to the polymer molecular mobility. The relationship between mechanical properties and secondary (subglassy) relaxation processes has been studied in a number of polymers (for review, see ref. 14). It was concluded that the general concept that secondary relaxation processes

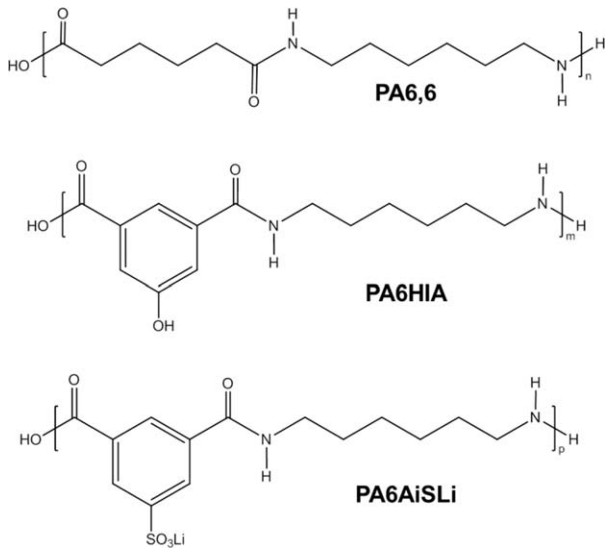

Figure 1. PA6,6, PA6HIA, and PA6AISLi chemical structures.

corresponding to localized motions within the chain backbone generally leads to an increase of impact strength, because it allows increasing considerably the dissipated energy.[15] This was mostly established using fracture propagation tests, in which the critical stress intensity factor, or fracture toughness (expressed in MPa $m^{1/2}$), is measured.[16]

The impact properties of PA6,6, namely the variation of the resilience with temperature, were described by Kohan.[1] It was observed that, starting form low temperatures, the resilience increases slightly as temperature approaches the brittle-tough transition temperature $T_{B/T}$. At $T_{B/T}$, the resilience rapidly increases with temperature until a ductile material is obtained. Moreover, Gaymans *et al.*[17] have studied the effect of water on the brittle-tough transition temperature $T_{B/T}$ in Polyamide 6 (PA6) and the relationship of this transition temperature with the glass transition temperature T_g. They observed that the $T_{B/T}$ is shifted toward lower temperatures when water is absorbed in the samples and that the drop on the $T_{B/T}$ induced by water is similar to that of the glass transition temperature T_g. Both transitions thus seem to follow the same trend.

In this article, we shall not put too much emphasis on the absolute values of impact strength (resilience) nor compare quantitatively the values obtained in different samples. Indeed, such a comparison may depend significantly on the crystalline morphology and on chain length distributions if the various samples. Rather, we put the emphasis on the temperature variation of impact properties. The objective is to investigate the possible relationship between impact strength properties and the polymer mobility in the amorphous phase.

Few studies in the literature deal with the relationship between molecular mobility and the mechanical properties of polyamides *per se*. Indeed, both temperature and/or solvent content modify the molecular mobility of the amorphous phase of polyamides. It is then of crucial importance to study and understand the role of the amorphous phase on the mechanical properties and how the mechanical properties of PA6,6 are affected by modifying the molecular mobility. In order to obtain PA6,6 samples having different molecular mobility states, two ways were considered herein: modifying PA6,6 by adding additives or comonomers; conditioning polyamide samples at different hygrometry levels, since PA6,6 T_g decreases significantly in presence of water (plasticization effect).[12,18–31] The yield stress (σ_Y) and Young's modulus (E) measured by tensile tests as well as the brittle-tough transition temperature ($T_{B/T}$) measured by Charpy impact tests are assessed for such PA6,6 samples. The relaxation processes were characterized by dynamical mechanical analysis (DMA) and broadband dielectric spectroscopy (BDS). The relationship between impact properties and PA6,6 molecular mobility is then discussed.

EXPERIMENTAL

Materials and Sample Conditioning

Five PA6,6-based materials, namely two PA6,6-based copolymers, two PA6,6 formulations additivated with alkyl-phenolic resins and a neat PA6,6 acting as reference, were considered. The two copolymers PA66/6HIA and PA66/6AISLi, supplied by Solvay, were obtained by copolycondensing 95 mol % adipic acid and 5 mol % of either isophthalic acid-based phenol (HIA) or isophthalic acid-based Lithium salt (6AISLi) with hexamethylene diamine. The resulting copolymers possess aromatic rings in their backbone structures, which rigidify the polymer. The structures of PA6HIA and PA6AISLI monomeric units are shown in Figure 1. The obtained copolyamides are hereafter named HIA (PA66/6HIA) and AISLI (PA66/6AISLi).

The nonfilled, nonadditivated Solvay-grade PA6,6 used as reference (hereafter denoted as REF) has a molecular mass M_n of about 15 kg mol^{-1} and an index of polydispersity of about 2. The alkyl-phenolic resins used as additives in PA6,6 formulations (developed by Solvay) were phenyl-laurylaldehyde (LA) and phenyl-heptanaldehyde (HA) oligomers. Their molecular structure is shown in Figure 2(a). Their degree of polymerization x is of order 8–10.

These additives might be able to bond to PA6,6 amide groups via the phenol functions. The H-bonds formed between the phenol of the additives and the amide groups in polymer chains are supposed to be stronger than those formed between amide groups, potentially inhibiting part of the absorption sites for polar solvents, as it was shown by *ab initio* molecular simulations.[32] Moreover, the presence of lateral alkyl chains –R might induce an increase on the molecular mobility through steric effects, which would be beneficial for impact strength

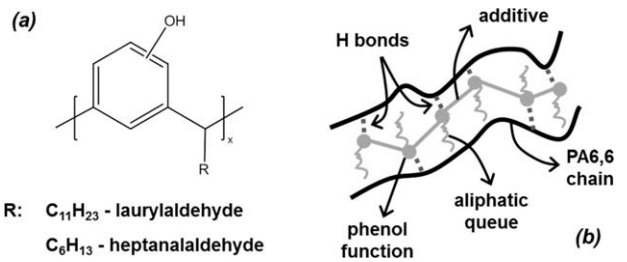

Figure 2. (a) Alkyl-phenolic resin chemical structure. (b) Interactions between PA6,6 and the resins.

Table I. Water Intake after RH50 and RH100 conditioning for the Studied formulations

	Water intake (% wt)	
Sample	RH50	RH100
REF	3.0	8.0
10LA	2.7	7.1
10HA	2.6	7.4
HIA	3.1	8.0
AISLI	3.4	11.6

properties. These interactions are schematically represented in Figure 2(b). The additivated PA6,6 materials were obtained by compounding 10 wt % of either LA or HA with the REF neat Solvay-grade PA6,6 using a Leistritz extruder (L/D ratio 33, throughput 10 kg/h). The obtained additivated formulations are hereafter denoted 10LA (PA6,6 + 10 wt % LA) and 10HA (PA6,6 + 10 wt % heptanalaldehyde). The formulations were injection-molded into tensile and impact strength specimens with an Arburg injection press. The dimensions of the tensile and impact strength specimens were 150 × 10 × 4 mm^3 and 80 × 10 × 4 mm^3, respectively (ISO-527 and ISO-157 norms). The specimens were dried for 4 days at 90 °C under vacuum afterwards, the resulting specimens being labeled as "dry" samples. Some of the dry specimens were then conditioned in a humid atmosphere: to obtain a 50% hygrometry level (RH50) conditioning, samples were put in a conditioning oven at 70 °C and RH63 for 2 weeks and then placed in a unit with a controlled atmosphere at 23 °C and RH50 until sorption equilibrium was reached. To obtain a 100% hygrometry level conditioning (RH100), the specimens were immersed in water at 80 °C and weighed periodically until sorption equilibrium was reached (which took ca. 4 days). The specimen were then stored in water-tight conditioning. The water intakes at sorption equilibrium for all materials (referred to the total weight of material) are listed in Table I.

It is effectively observed that LA and HA additives partly inhibit global water sorption. However, when referred to the PA6,6 content in the samples, which represents 90 wt % of the additivated materials, the water intake is not significantly affected. However, as might be expected, introducing ionic moieties in AISLi increases water sorption.

Characterization Methods

The crystalline ratios of the samples were obtained by Differential Scanning Calorimetry (DSC) measurements performed at 10 °C/min, with ΔH_f^0, the heat of melting of a 100% crystalline PA66, taken as 188.4 J/g for all samples.[5] Table II shows the measured crystalline ratios obtained by DSC, referred either to the total mass of sample or to the effective PA66 mass content. Table II shows that the overall crystalline ratios of the four modified polyamides are slightly lower than that of REF. However, the fraction of PA6,6 moieties is lower in the modified formulations, PA6,6 a priori being the only component of the formulations which is able to crystallize. Therefore, crystallinity indices were corrected to refer to the amount of PA6,6 groups in each sample. Corrected values are reported in column 3 in Table II. The corrected crystalline ratios in the copolymer samples (HIA, AISLI) are relatively similar to that of REF. This means that introducing 5 mol % aromatic comonomers does not affect the crystalline fraction of PA6,6 chain segments significantly. In the case of 10LA and 10HA, it seems that the presence of the additives slightly increases crystalline ratios (referred to PA6,6 content), but the values remain close to that of REF. These results insure that the various samples may be considered to be comparable as regards their overall crystallinity. However, for a given crystalline fraction, differences in the crystalline morphology (number and size of spherulites, crystalline perfection) may still significantly affect the mechanical properties.

Note also that, if it is assumed that only PA6,6-type monomers crystallize, both additives and/or phthalic-based comonomers shall be expelled in the amorphous phase. As a result, the actual additive or phthalic modifier fraction in the amorphous phase shall be a little higher than the overall nominal content indicated above.

The molecular mobility of the dry and water-conditioned samples was assessed by Modulated DSC (MDSC), BDS, and DMA. MDSC measurements were conducted with a TA Q2000 instrument in the temperature-modulated mode from −50 to 140 °C at 3 °C/min with a temperature modulation of ±2 °C every 60 s. The glass transition temperatures T_g was taken at the inflexion point of the heat capacity jump. BDS measurements were performed with a Novocontrol Alpha Analyser and a Quatro temperature control system. 300 μm-thick samples were cut in disks of diameter 2 cm placed in between electrodes, and then heated from −150 to 200 °C with 4 °C steps, each temperature step being scanned at 46 frequencies ranging from 0.01 to 10^7 Hz. The software WinFit from Novocontrol was used to analyze DBS data for both the β and α relaxations in all samples as a function of temperature.

DMA measurements were carried out with a TA Q800 analyzer. Impact specimens were used to characterize the mechanical relaxations, using the three-point bending method. The measurements were carried out in a closed furnace. The samples were cooled down to −150 °C and heated up to 200 °C at 2 °C/min. The frequency of the applied stress was fixed at 1 Hz. The value of T_α was taken at the inflection point on the drop of the dynamic elastic modulus E'.

Table II. PA66 Mass-Corrected Crystalline Ratios (XC and XC-PA66, Respectively) Obtained by DSC in the Dry Samples

Sample	X_C (%)	$X_{C\text{-}PA66}$ (%)
REF	34.1	34.1
10LA	32.5	36.1
10HA	32.8	36.4
HIA	32.3	34.3
AISLI	30.9	33.3

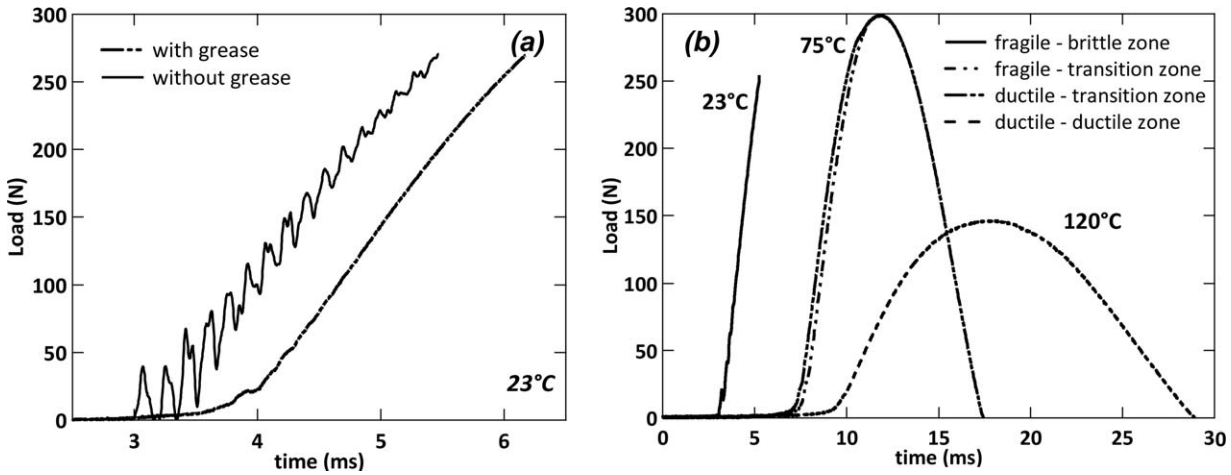

Figure 3. Impact force as a function of time for (a) a PA6,6 sample at room temperature with and without damping silicon grease and (b) PA6,6 samples at different temperatures highlighting the brittle and tough behavior during Charpy impact tests.

The Young's modulus E and the yield stress σ_Y of the studied samples were obtained by tensile experiments carried out with a Zwick/Roell Z020 machine equipped with a temperature chamber and a laser extensometer. The crosshead speed was set at 1mm/min ($\dot{\varepsilon} = 3 \times 10^{-4}$ s^{-1}) for the first 0.5% of deformation and at 5mm/min ($\dot{\varepsilon} = 2 \times 10^{-3}$ s^{-1}) further on. Dry samples only were measured at 23, 45, 60, 90, and 120 °C.

An instrumented Charpy impact setup was used to obtain the impact strength and the $T_{B/T}$ of the dry and water-conditioned samples.[16] The energy of the hammer was 7.52 J and the samples were hit at a speed $v_{impact} = 1$ m/s. Samples were notched with a notch depth of 2 mm and a radius $r_{notch} = 0.1$ mm (which corresponds to a deformation rate v_{impact}/r_{notch} of order of magnitude 10^4s^{-1}). A custom-made software was used to acquire and analyze the obtained impact curves. Impact strength tests were conducted from −60 to 150 °C so as to obtain the $T_{B/T}$ of the studied samples. The samples temperature was estimated to remain roughly constant during the impact tests (measured loss of 1 °C of the sample's temperature with a thermocouple during the few second testing time). The instrumented impact setup measures the impact force as a function of time. Silicon grease was used as mechanical filter to damp elastic oscillations during impact, which introduce some noise in the force signal. Figure 3(a) shows that using silicone grease yields a disappearance of the impact noise without affecting the shape of the curve, allowing a better analysis. Furthermore, Figure 3(b) shows the impact curve shapes obtained at 23, 75, and 120 °C for neat PA6,6, as representative examples. This graph highlights the evolution of impact curves when going from the brittle to the tough behavior, which allows obtaining the brittle-tough transition temperature $T_{B/T}$.[16] The impact strength (in J/m^2) is defined as the energy used to fracture the material (the area under the impact force curve), divided by the fracture surface area.

The water conditioning states of the samples were considered to remain constant during the impact testing. Indeed, samples are kept 15 min at the set temperature for equilibration prior to impact testing. The laboratory atmospheric conditions are of a controlled temperature (23 °C) and hygrometry (RH50). In the case of the dry samples, the temperature equilibration time is too small to induce significant water intake. Concerning the RH50-conditionned samples, this temperature equilibration time is also too small to induce a significant loss of water by the samples. Finally, in the case of the RH100-conditioned materials, no further water intake or loss is supposed to occur during temperature conditioning.

RESULTS AND DISCUSSION

Molecular Mobility

The secondary β (rotation of amide functions within the chains) and main (α or glass transition) relaxations[1] of the studied PA6,6 formulations have been characterized by BDS over broad frequency and temperature ranges. The β transition was determined by fitting isothermal frequency curves of the complex permittivity ε^* with a Cole-Cole model $\varepsilon^* = \varepsilon' + i\varepsilon'' = \varepsilon_\infty + \Delta\varepsilon/\left(1+\left(i\omega\tau_\beta\right)^m\right)$,[33] in which the exponent m ($0 < m < 1$) describes a symmetric broadening of the molecular relaxation process (related to the relaxation time distribution).[34] In the region of the α relaxation, ε^* frequency curves were fitted with the Havriliak–Negami model $\varepsilon^* = \varepsilon' + i\varepsilon'' = \varepsilon_\infty + \Delta\varepsilon/(1+(i\omega\tau_\alpha)^m)^n$, where n ($mn \leq 1$) describes a nonsymmetrical broadening of the molecular relaxation process, as is often the case for glass transition in polymer.[33–35]

Several issues occur when characterizing relaxations in polyamides by BDS. The range in which the permittivity can be fitting to the α relaxation is limited because this relaxation is accompanied by a strong increase of the sample conductivity. Alternatively, τ_α may be determined from the maximum of the loss permittivity and/or the loss modulus $M^* = 1/\varepsilon^*$ in isochronal curves. Although it is less precise, this method was preferred because it provides relaxation times over a larger temperature range. The loss modulus representation is less sensitive to contributions from sample conductivity and gives a well-defined peak. The values obtained from the loss modulus are shifted (by about 15–20 °C at a given frequency) with respect to the values obtained from the loss permittivity but allow double checking of the latter.[36]

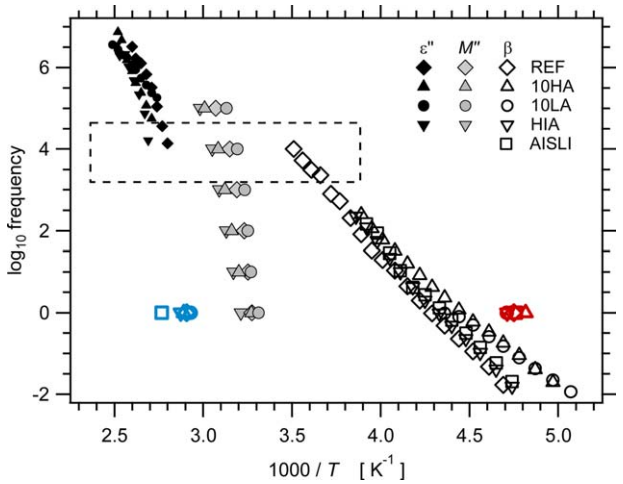

Figure 4. Molecular relaxation map for the secondary β and main α relaxations for the modified and nonmodified polyamides in the dry state. Black symbols refer to data for the α relaxation obtained from isothermal ε^* frequency curves, white symbols refer to β relaxation data obtained in the same way. Gray symbols refer to a relaxation data obtained from isochronal dielectric modulus M^* curves. Red (resp. blue) symbols are from DMA data at 1 Hz for the β (resp. α) relaxation. The range of typical deformation rate in Charpy impact tests is highlighted by a dashed rectangle. [Color figure can be viewed in the online issue, which is available at wileyonlinelibrary.com.]

However, in the presence of water, care must be taken that the α relaxation temperature occurs well below water evaporation. In addition, regarding the β relaxation, it was shown that, in the presence of water, this relaxation may become complex, showing two partially overlapping peaks. These peaks have been tentatively related to motions of bonded amide groups and motions of water molecules.[19,36]

The relaxation maps (the log of the frequency as a function of the inverse temperature) obtained from the analysis of dielectric spectra measured for all dry samples are shown in Figure 4. The obtained range of α relaxation measured from isothermal ε^* curves is limited due to sample conductivity at low frequency, as explained before. The α relaxation in AISLI could not be obtained at all in this way, as the polymer was found to be highly conductive at high temperatures. This is due to the presence of ionic lithium sulfate groups (Li^+ RSO_3^-) in the polymer structure (Figure 1). Given that the lithium cation is very labile, the polymer conductivity increases dramatically with temperature as polymer chains, and thus the lithium sulfate functions, gain mobility.

Figure 4 shows that the curves for the α relaxation obtained by the two methods described above are indeed roughly parallel but shifted in frequency. When comparing with the data obtained by DMA at 1 Hz (red and blue symbols in Figure 4), some differences appear. For the β relaxation, the difference may be due to the fact that BDS measurements make use of the permittivity, which is a compliance, whereas mechanical data are from the modulus G^*. The difference then comes from the difference between relaxation and retardation times. For the α relaxation, the DMA data correspond well to the extrapolated black symbols, as expected (α relaxation is measured in DMA by the inflexion point of G', not from the G'' maximum). Then, MDSC yields T_g values which compare also well to other relaxation data for the studied formulations, as shown in Table III. These measurements confirm that the modified formulations indeed have different molecular mobility states.

Table III. T_g and T_α@1Hz Measured by MDSC, BDS, and DMA for the Dry Samples

Sample	T_g (°C) DSC	T_α@1 Hz (°C) BDS	T_α@1 Hz (°C) DMA
REF	71	68	71
10LA	62	64	69
10HA	67	67	73
HIA	77	74	75
AISLI	91	90	89

Table IV shows the temperature of the β and α relaxations at 1 Hz in all samples, conditioned dry, at RH50 and at RH100. Both relaxation processes are strongly affected by water intake. The β relaxation temperatures were measured by DMA, specifically for water-conditioned samples. Indeed, it has been shown that multiple dielectric relaxation processes appear in the region of the β relaxation in the presence of water. These processes have been attributed to the motions of water molecules forming hydrogen bonds with amid groups, as well as to the reorientation of amide groups themselves.[19,36] Thus, we consider that it is preferable to consider the β relaxation measured by DMA, as being representative of a process related to the polymer mobility itself.

Tensile Properties

The yield stress σ_Y and the Young's modulus E were determined from tensile measurements conducted at different temperatures. The different samples were compared at a given state of molecular mobility that was defined by the temperature difference between the T_g and the tensile experiment temperature ($T - T_g$). Results are shown in Figures 5 and 6. σ_Y's values are reported at temperatures below T_g only, since above T_g the materials do not show a properly defined yield stress. Conversely, a Young's modulus can still be defined close to and slightly above T_g, even though the polymer starts to behave as a viscoelastic material.

Table IV. Temperatures of α and β Relaxation Processes Measured by DMA at 1 Hz at Different Water Conditioning

	T_β (°C)			T_α (°C)		
Sample	Dry	RH50	RH100	Dry	RH50	RH100
REF	−62.5	−79,5	−97,4	71	19,9	−15,5
10LA	−60.7	−73,4	−81,5	68.4	21,9	−15,0
10HA	−65.4	−79,8	−99,9	73	29,1	−17,8
HIA	−60.8	−78,9	−99,0	75	29,6	−12,0
AISLI	−63	−78,1	−102,5	88.5	35,2	−18,4

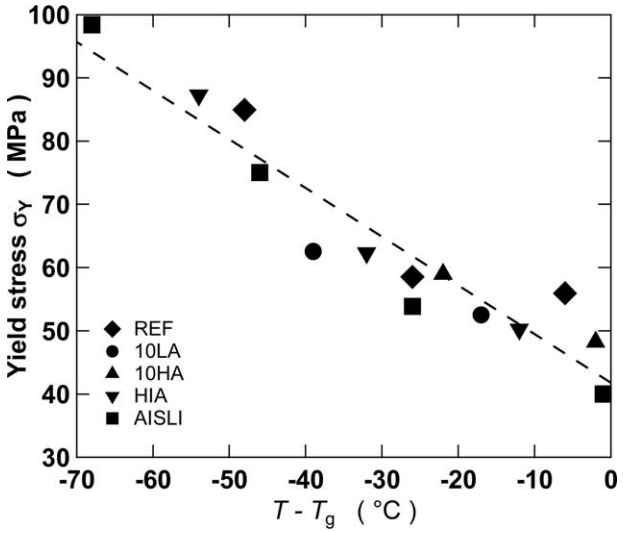

Figure 5. Yield stress σ_Y below T_g plotted as a function of $T-T_g$ (same molecular mobility) for dry samples. The dashed line corresponds to the linear fit $\sigma_Y = -0.78(T-T_g)+41.4$.

Figure 5 shows that there is a clear correlation between the yield stress values σ_Y and the molecular mobility for all the studied PA6,6-based materials over a wide range of molecular mobility states. In other words, this would mean that the yield stress σ_Y for any of the studied samples has a similar value at the same state of molecular mobility. However, σ_Y values are relatively scattered, due to experimental uncertainties. Note however that in semicrystalline materials, the yield stress is very sensitive to the crystalline morphology, and one may perhaps infer a general tendency of the data for AISLI, which is slightly less crystalline (see Table II), to be roughly 5 MPa below the data for other samples.

The measured Young's moduli E were then plotted as a function of $T-T_g$ (same state of molecular mobility) as shown in Figure 6.

As seen in Figure 6 the Young's moduli E considered at a given molecular mobility state can differ significantly from one formulation having a different molecular mobility state to another, the variation of the molecular mobility being linked to the chemical structure of the samples. However, all studied formulations have relatively similar Young's modulus curves, and it is difficult to discriminate a general trend in the differences between these curves. The drop of Young's modulus for AISLI seems to extend over a temperature range broader than for other samples. The drop in the dynamic elastic modulus E' associated to the α relaxation process measured by DMA plotted in Figure 7 shows as well a similar trend for all samples, with a somehow broader temperature variation for AISLI. This difference might be the signature of the variation of the intermolecular interactions within PA6,6 chains induced by the presence of PA6AiSLi comonomers in the neat matrix.

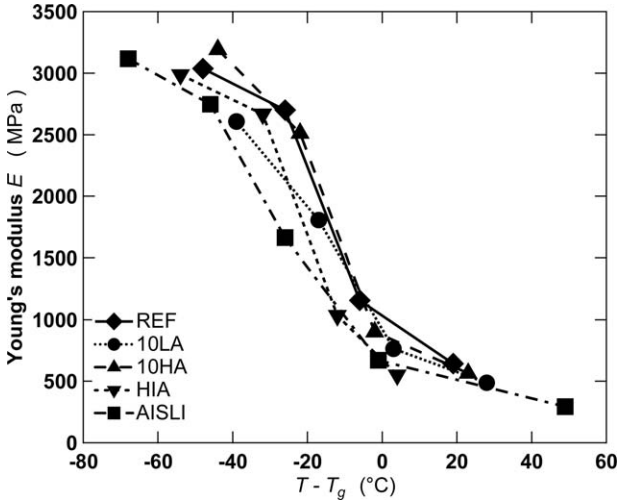

Figure 6. Young's moduli E as a function of $T-T_g$ (same molecular mobility) for dry samples.

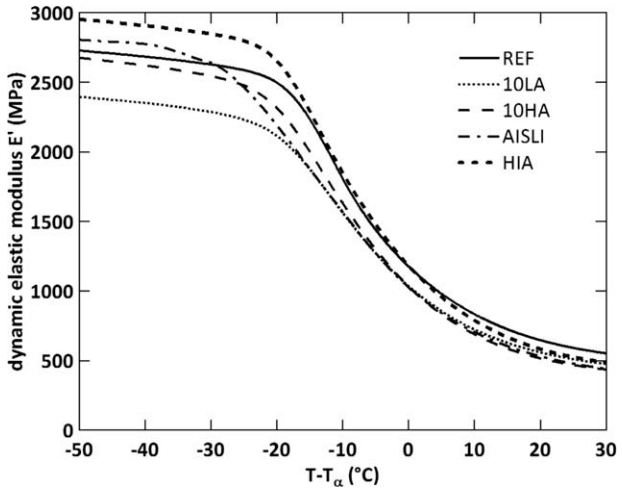

Figure 7. Dynamic elastic modulii E' obtained by DMA as a function of $T-T_\alpha$ (same molecular mobility) for dry samples.

Impact Strength Properties

Impact strength tests were conducted on dry and water-conditioned reference and modified materials as described in the experimental section. Figure 8 shows the impact strength J as a function of temperature (brittle-tough transition curves) for the five studied formulae in the (a) dry, (b) RH50, and (c) RH100 conditioning states respectively. In all cases, the curves show a well-defined transition from brittle failure at low temperature, where the impact strength (or resilience) is of order $J_0 \cong 2$ to 5 kJ/m^2, to ductile behavior at high temperature, where the impact strength (referred to the actual fracture surface created in the sample (samples do not break completely in this regime) is of order $J_\infty \cong 60$ kJ/m^2. To determine precisely the brittle-tough transition temperatures $T_{B/T}$, the curves were adjusted to a sigmoidal shape $J(T)=J_0+(J_\infty-J_0)/\ (1+\exp\left(\left(T_{B/T}-T\right)/w_0\right))$. Examples of such adjustements are shown in Figure 8(a). Note that prior to reach the transition temperature on the low temperature side, the impact strength increases progressively from 2-5 to 10-15 kJ/m^2 within a temperature range of about 25 °C. This increase may be due to increased ability of the material to dissipate energy, as will be discussed below. The general shapes of the curves are qualitatively similar for all samples and all water conditioning states. The main difference lies in the transition temperature. The $T_{B/T}$ values for the studied

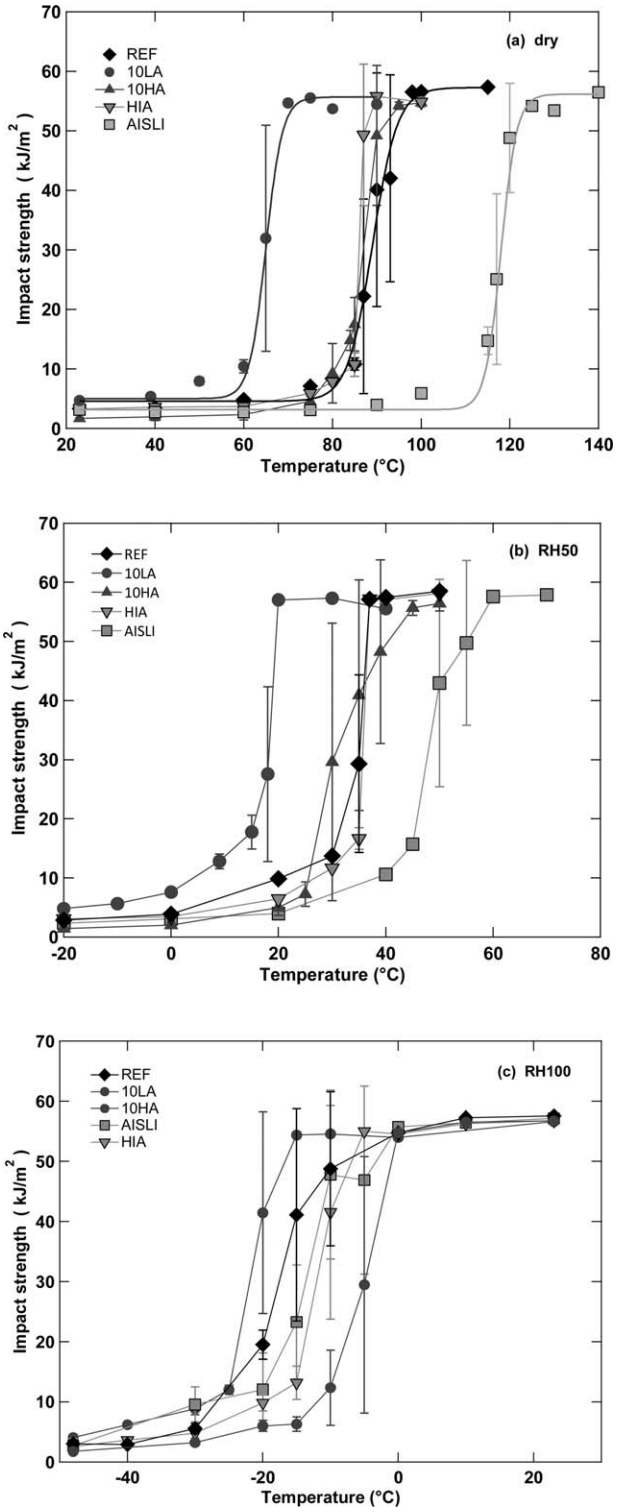

Figure 8. Brittle-tough transition curves at (a) the dry state, (b) RH50-conditioning, and (c) RH100-conditioning. In Graph (a), curves in between points for REF, 10LA, and AISLI samples are sigmoidal adjustments of data.

materials in the dry state and conditioned at RH50 and RH100, determined from the inflexion points in the curves shown in Figure 8, are reported in Table V.

Table V. $T_{B/T}$ Transition Temperatures (in °C) Obtained in the Dry State, RH50-, and RH100-Conditioning for the Studied Materials

Formulation	Dry	RH50	RH100
REF-I	88	36	−17
10LA-I	65	18	−22
10HA-I	87	32	−5
HIA-I	86	36	−12
AISLI-I	118	47	−12

DISCUSSION

Different mechanisms may occur as a crack propagates, for example, during impact tests. These mechanisms depend on the temperature and mobility state of the polymer. We are thus interested on the relationship between molecular mobility and impact strength properties. It is known that the secondary relaxations have an important impact on the brittle-tough behavior of fully amorphous polymers (i.e., the $T_{B/T}$ lies between the T_g and the foremost secondary relaxation).[14] However, in semi-cristalline materials, the brittle-tough transition depends mostly on the T_g, as the polymer can still maintain a certain level of mechanical properties beyond the glass transition since the cristallites act as material reinforcements. Thus, we shall investigate here the relationship between the brittle-tough transition and the relaxation processes. The brittle-tough transition temperatures $T_{B/T}$ determined from the curves in Figure 8 are plotted as a function of the T_g in Figure 9 for the different samples that were either dry or conditioned at different hygrometry levels.

Figure 9 shows that the $T_{B/T}$'s of all the samples seem to follow a linear relationship as a function of the T_g's of all the materials and conditioning states, which would mean that, for a given polyamide sample, its brittle-tough transition depends directly on its molecular mobility state as determined by its α or glass

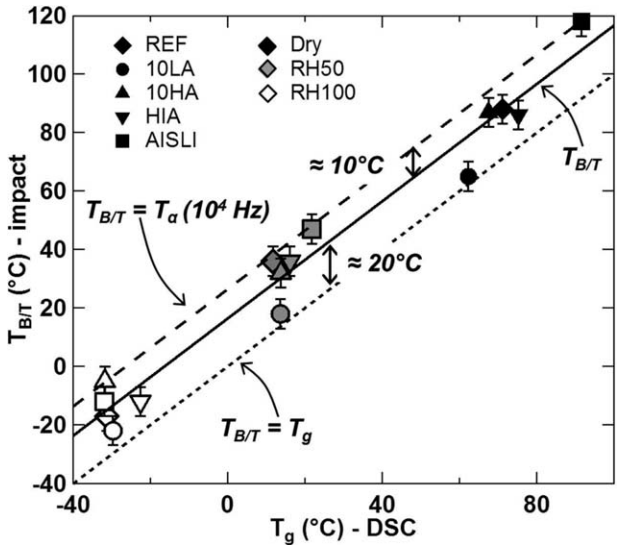

Figure 9. $T_{B/T}$ plotted as a function of T_g for the modified and nonmodified polyamides (dry, RH50, and RH100).

transition temperature. However, the $T_{B/T}$'s are very far away from T_β as illustrated in Figures 10 and 11. Indeed, it is observed in Figure 4 that at a frequency of 10^4 Hz, corresponding to the estimated order of magnitude of the deformation rate in Charpy impact tests, the sample $T_{B/T}$'s seem to be closer to T_α (ca. 90 to 100 °C) than to T_β (ca. 10 °C) at this same frequency. This result agrees very well with the relationship between T_g and $T_{B/T}$ shown above. Nevertheless, a contribution from the β relaxation on the increase of impact resistance, which is observed prior to the onset of brittle-tough transition (see Figure 8) cannot be excluded.

It is observed that the $T_{B/T}$ values are higher than the T_g values, with an average upward shift of 15 °C between the $T_{B/T}$ and the T_g. This upward shift could be explained by the fact that impact tests are performed at high deformation rates (of the order of 10^4 s^{-1}). Instead of comparing $T_{B/T}$ values to T_g, (as mesured by DSC) or to T_α (as measured by DMA at 1 Hz), it should perhaps be compared to the T_α measured at a frequency of order 10^4 Hz, comparable to the effective deformation rate in impact tests. As explained above, due to difficulties inherent to BDS measurements in the presence of water, it was not possible to obtain reliable values of T_α at 10^4 Hz for all samples at all humidity conditioning conditions. It is observed in Figure 4 that shifting the frequency from 1 to 10^4 Hz rouhgly shifts T_α by about 25 °C, which semiquantitatively seems to correspond to the observed difference between $T_{B/T}$ and T_g.

On the more fundamental side, the nature of the glass transition in polymers, in relation to the onset of molecular mobility, is still an actively debated subject.[37] Specifically, recent experimental works have shown how the molecular mobility is affected by stress, thus leading to a decrease of T_g in the presence of stress.[38–40] Specifically, the yield stress behavior, characterized by the onset of flow beyond a certain stress level, has been interpreted as due to this plasticization effect (decrease of T_g) under stress. Altogether, the results presented here, specifically in Figure 9, indicate that the large scale mobility in the amorphous phase provided by the onset of glass transition, is necessary to observe the onset of locally ductile fracture behavior which corresponds to the brittle-tough transition in impact tests.

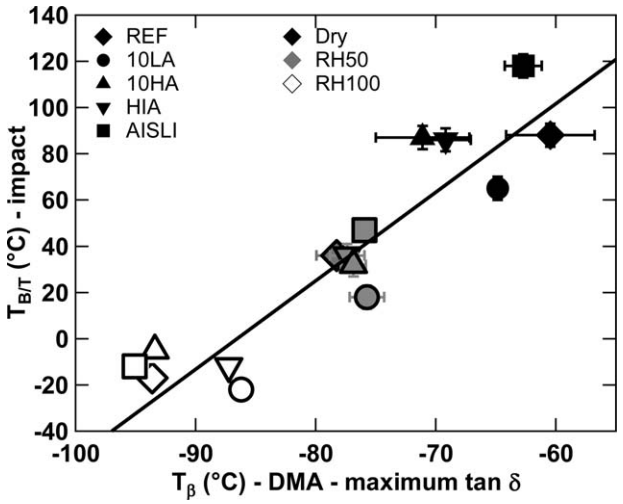

Figure 10. $T_{B/T}$ plotted as a function of T_β measured by DMA at 1 Hz for the reference and modified polyamides (dry, RH50 and RH100).

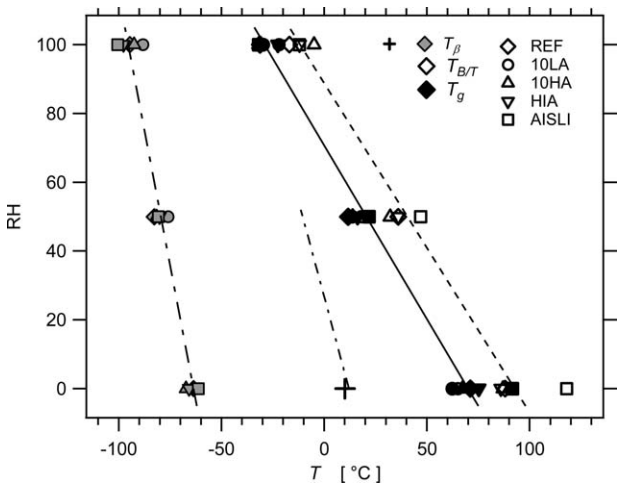

Figure 11. Comparison of the brittle-tough transition temperature $T_{B/T}$ with the glass transition temperature T_g and the β transition temperature, for the different mobility states obtained by varying the water conditioning. The cross locates the value of T_β measured by BDS at 10^4 Hz, with its hypothetical variation with water conditioning indicated by a dashed-dotted line.

CONCLUSION

In this work, the impact strength properties of a series of semicrystalline PA6,6-based polymers were studied by using instrumented Charpy impact tests on a broad temperature range. The impact strength properties were studied in the dry and water-conditioned polymers at 50 and 100% humidity. Water conditioning induces large changes in the molecular mobility of the amorphous phase of the materials, as reflected in the large variation of the T_g of the materials. The brittle-tough transition temperatures $T_{B/T}$ were compared with the T_g's. It was observed that there is a linear dependence of $T_{B/T}$ with T_g, which means that for the studied semicrystalline polyamides 6,6-based materials, their brittle-tough transition depends directly on their large-scale molecular mobility state. Furthermore it was observed that there was a temperature shift upwards between the T_g and the $T_{B/T}$ because impact strength tests are carried out at high deformation rates and should be compared with the T_g or T_α at this loading frequency.

ACKNOWLEDGMENTS

The authors thank Hélène Coste and Frédéric Brun (Solvay) for their help with tensile and impact strength experimental setups, Stéphane Jéol and Daniel Duchêne (LSPP Laboratory, Solvay) for the synthesis of the polymers. They thank Caroll Vergelati (Solvay) for fruitful discussions. They acknowledge the funding of the broadband dielectric setup by the GRAND LYON metropolitan council.

REFERENCES

1. Kohan, M. L. Nylon Plastics Handbook; Carl Hanser Verlag: Munich, **1995**.

2. Yeh, J. T.; Chang, S. S.; Yao, H. T.; Chen, K. N.; Jou, W. S. *J. Mater. Sci.* **2000**, *35*, 1321.
3. Huang, J. J.; Keskkula, H.; Paul, D. R. *Polymer* **2004**, *45*, 4203.
4. Huang, J. J.; Keskkula, H.; Paul, D. R. *Polymer* **2006**, *47*, 639.
5. Huang, J. J.; Keskkula, H.; Paul, D. R. *Polymer* **2006**, *47*, 3505.
6. Garcia, D.; Starkweather, H. W. *J. Polym. Sci.* **1985**, *23*, 537.
7. Bessler, E.; Bier, G. *Makromol. Chem.* **1969**, *122*, 30.
8. Schroeder, L. R.; Cooper, S. L. *J. Appl. Phys.* **1976**, *47*, 4310.
9. Starkweather, H. W.; Moore, G. E.; Hansen, J. E.; Roder, T. M.; Brooks, R. E. *J. Polym. Sci.* **1956**, *21*, 189.
10. Bureau, M. N.; Denault, J.; Cole, K. C.; Enright, G. D. *Polym. Eng. Sci.* **2002**, *42*, 1897.
11. Starkweather, H. W.; Brooks, R. E. *J. Appl. Polym. Sci.* **1959**, *11*, 236.
12. Miri, V.; Persyn, O.; Lefebvre, J. M.; Séguela, R. *Eur. Polym. J.* **2009**, *45*, 757.
13. Shan, G.; Yang, W.; Yang, M.; Xie, B.; Feng, J.; Fung, Q. *Polymer* **2007**, *48*, 2958.
14. Monnerie, L.; Halary, J. L.; Kausch, H. H. *Adv. Polym. Sci.* **2005**, *187*, 215.
15. Heijboer, J. *J. Polym. Sci.* **1968**, *16*, 3755.
16. Kausch, H. H. Polymer Fracture, 2nd ed.; Springer-Verlag: Berlin Heidelberg, **1987**.
17. Gaymans, R. J.; Borggreve, R. J. M.; Spoelstra, A. B. *J. Appl. Polym. Sci.* **1989**, *37*, 479.
18. Rios de Anda, A.; Fillot, L. A.; Rossi, S.; Long, D. R.; Sotta, P. *Polym. Eng. Sci.* **2011**, *51*, 2129.
19. Laurati, M.; Sotta, P.; Long, D. R.; Fillot, L. A.; Arbe, A.; Alegría, A.; Embs, J. P.; Unruh, T.; Schneider, G. J.; Colmenero, J. *Macromolecules* **2012**, *45*, 1676.
20. Murthy, N. S.; Stamm, M.; Sibilia, J. P.; Krimm, S. *Macromolecules* **1989**, *22*, 1261.
21. Puffr, R.; Sebenda, J. *J. Polym. Sci. C* **1967**, *16*, 79.
22. Iwamoto, R.; Murase, H. *J. Polym. Sci. Part B: Polym. Phys.* **2003**, *41*, 1722.
23. Vinken, E.; Terry, A. E.; van Asselen, O.; Spoelstra, A. B.; Graf, R.; Rastogi, S. *Langmuir* **2008**, *24*, 6313.
24. Dixon, D. A.; Dobbs, K. D.; Valentini, J. J. *J. Phys. Chem.* **1994**, *98*, 13435.
25. Lim, L. T.; Britt, I. J.; Tung, M. A. *J. Appl. Polym. Sci.* **1999**, *71*, 197.
26. Starkweather, H. W.; Barkley, J. R. *J. Polym. Sci. Part B: Polym. Phys.* **1981**, *19*, 1211.
27. Auerbach, I.; Carnicom, M. L. *J. Appl. Polym. Sci.* **1991**, *42*, 2417.
28. Laredo, E.; Grimau, M.; Sánchez, F.; Bello, A. *Macromolecules* **2003**, *36*, 9840.
29. Reimschuessel, H. K. *J. Polym. Sci. Polym. Chem.* **1978**, *16*, 1229.
30. Laredo, E.; Hernandez, M. C. *J. Polym. Sci. Part B: Polym. Phys.* **1997**, *35*, 2879.
31. Le Huy, H. M.; Rault, J. *Polymer* **1994**, *35*, 136.
32. Hartikainen, J.; Lehtonen, O.; Harmia, T.; Lindner, M.; Valkama, S.; Ruokolainen, J.; Friedrich, K. *Chem. Mater.* **2004**, *16*, 3032.
33. McCrum, N. G.; Read, B. E.; Williams, G. Anelastic and Dielectric Effects in Polymer Solids; Dover: New York, **1991**.
34. Kremer, F.; Schönhals, A. Broadband Dielectric Spectroscopy; Springer: Berlin, **2003**.
35. Havriliak, S.; Negami, S. *Polymer* **1967**, *8*, 161.
36. Preda, F. M.; Alegría, A.; Bocahut, A.; Fillot, L. A.; Long, D. R.; Sotta, P. *Macromolecules* **2015**, *48*, 5730.
37. Xu, B.; McKenna, G. *J. Chem. Phys.* **2011**, *134*, 124902.
38. Lee, H. N.; Paeng, K.; Swallen, S. F.; Ediger, M. D. *Science* **2009**, *323*, 231.
39. Bending, B.; Christison, K.; Ricci, J.; Ediger, M. D. *Macromolecules* **2014**, *47*, 800.
40. Kalfus, J.; Detwiler, A.; Lesser, A. J. *Macromolecules* **2012**, *45*, 4839.